2010 IEEE International Conference on Robotics and Automation
Anchorage Convention District
May 3-8, 2010, Anchorage, Alaska, USA

A Visual-Servoing Scheme for Semi-Autonomous Operation of an Underwater Robotic Vehicle Using an IMU and a Laser Vision System

George C. Karras, Savvas G. Loizou and Kostas J. Kyriakopoulos

Abstract— **This paper presents a visual servoing control scheme that is applied to an underwater robotic vehicle. The objective of the proposed control methodology is to provide a human operator the capability to move the vehicle without loosing the target from the vision system's field of view. On-line estimation of the vehicle states is achieved by fusing data from a Laser Vision System (LVS) and an Inertial Measurement Unit (IMU) using an asynchronous Unscented Kalman Filter (UKF). A controller designed at the kinematic level, is backstepped into the dynamics of the system, maintaining its analytical stability guarantees. It is shown that the under-actuated degree of freedom is input-to-state stable and an energy based shaping of the user input with stability guarantees is implemented. The resulting control scheme has analytically guaranteed stability and convergence properties, while its applicability and performance are experimentally verified using a small Remotely Operated Vehicle (ROV) in a test tank.**

I. INTRODUCTION

Underwater vehicles usually operate in circumstances demanding dexterous operations and delicate motions, such as the inspection of ship hulls, propulsion system or other underwater structures. In most of these cases human intervention is essential for the mission success and the safety of the vehicle. Thus, semi-autonomous operation is the control mode of choice whether an operation entails challenging inspection and survey tasks. Depending on the mission's requirements, different sets of sensor suites are utilized for the robot's state estimation and the environmental perception. The vehicle's on board camera and the Inertial Measurement Unit (IMU) stand out as a particularly useful sensors for tasks concerning underwater inspection. On the one hand, the camera provides information of the vehicle's surrounding workspace, while on the other hand the IMU provides 3D linear accelerations and angular velocities.

In a typical direct teleoperation scenario, the operator based on the camera video feed, navigates the robot towards the inspection area and stabilizes or hovers the vehicle around a target of interest - usually a damaged area. Keeping this target inside the field of view is an essential, but a rather tricky undertaking. The operator must perform delicate moves and accurate manoeuvres, while dealing with strong currents, waves and also compensate for the ROV's tether.

Additionally, teleoperation becomes even more difficult, considering that most of the underwater vehicles (especially some small class ROVs), suffer from kinematic constraints, due to under-actuation along their sway axis. Hovering around a target can be accomplished only by fast and complex combinations of linear and angular velocity command inputs. This kind of teleoperation causes the target to oscillate inside the image frame, while in many cases the pilot fails to keep the target inside the camera's optical field. The result is a poor quality inspection video, while the mission has to be repeated several times to come up with a satisfactory result. A solution to this problem can be provided by implementing a semi-autonomous control scheme on the underwater robot.

The problem of keeping the target inside the field of view has been examined in the past, in robotic manipulators [1], cartesian robots [2], differential drive mobile robots [3], and underwater vehicles [4]. Also some interesting work has been done in [5], but all the above cases are mainly based on kinematic control laws or path planning techniques which do not incorporate the (nonlinear) dynamics of the system and their effect on the camera field of view.

In this paper a new switching visual servo control scheme is designed for semi-autonomous operation of an underwater vehicle that is underactuated along the sway axis. The proposed controller imposes a bounded trajectory around the center of a target, while guarantees that the target remains inside the camera's optical field. The design of the controller is based on feed-forwarding the dynamics of the system and back-stepping a Lyapunov based kinematic controller [6]. The complete state vector of the vehicle is obtained by asynchronously fusing data from a Laser Vision System (LVS) and an Inertial Measurement Unit (IMU) using an Unscented Kalman Filter (UKF). The human operator performs hovering tasks by simply providing high level commands by means of joystick lateral inputs. The difficult part of performing the necessary manoeuvres is left to the controller. In addition to the provided analytical guarantees, the methodology is assessed by a number of experiments that were carried out using an under–actuated 3 DOF ROV.

The rest of this paper is organized as follows: Section II gives an overview of the robot's kinematic and dynamic equations. Section III describe the state estimation using the LVS and the IMU. Section IV describes the control methodology, while Section V illustrates the efficiency of our approach through an experimental procedure. Eventually, Section VI concludes the paper.

G.C. Karras and K.J. Kyriakopoulos are with the Control Systems Lab, School of Mechanical Engineering, National Technical University of Athens,karrasg,kkyria@mail.ntua.gr

S.G. Loizou is with the School of Mechanical Engineering, Frederick University, Cyprus s.loizou@frederick.ac.cy

II. PRELIMINARIES

Generally an underwater vehicle is considered as a 6 DOF free body with position and Euler angle vector $\mathbf{n} = [x\ y\ z\ \phi\ \theta\ \psi]^T$. The body velocities vector is defined as $\mathbf{v} = [u\ v\ w\ p\ q\ r]^T$ where the components have been named according to SNAME as surge, sway, heave, roll, pitch and yaw respectively. The forces and moments vector acting on the body-fixed frame is defined as $\tau = [X\ Y\ Z\ K\ M\ N]^T$.

The general form of the dynamics of an underwater vehicle expressed in the body-fixed frame is given in matrix form by the equations below [7]:

$$\begin{aligned} &\mathbf{M}\dot{\mathbf{v}} + \mathbf{C}(\mathbf{v})\mathbf{v} + \mathbf{D}(\mathbf{v})\mathbf{v} + \mathbf{g}(\mathbf{n}) = \tau \\ &\dot{\mathbf{n}} = \mathbf{J}(\mathbf{n})\mathbf{v} \end{aligned} \tag{1}$$

where: $\mathbf{M} = \mathbf{M_{RB}} + \mathbf{M_A}$ is the inertia matrix for rigid body and added mass respectively, $\mathbf{C}(\mathbf{v}) = \mathbf{C_{RB}}(\mathbf{v}) + \mathbf{C_A}(\mathbf{v})$ is the coriolis and centripetal matrix for rigid body and added mass respectively, $\mathbf{D}(\mathbf{v}) = \mathbf{D_{quad}}(\mathbf{v}) + \mathbf{D_{lin}}(\mathbf{v})$ is the quadratic and linear drag matrix respectively, $\mathbf{g}(\mathbf{n})$ is the hydrostatic restoring force vector, τ, is the thruster input vector and $\mathbf{J}(\mathbf{n})$ is the Jacobian matrix transforming the velocities from the body-fixed to earth-fixed frame.

The vehicle used in this work is a 3 DOF VideoRay Pro ROV. It is equipped with three thrusters, which are effective only in surge, heave and yaw motion, meaning that the vehicle is under-actuated along the sway axis. The angles ϕ, θ and angular velocities p and q are negligible and we can consider them to be equal to zero. The ROV is symmetric about x - z plane and close to symmetric about y - z plane. Therefore, we can safely assume that motions in heave, roll and pitch are decoupled [7]. However in this paper we will be considering the coupling between surge, sway and roll that will be affecting the surge and sway motions since this is important for our task. Although the vehicle is not symmetric about x - y plane, heave motion can be considered decoupled from surge and sway because the vehicle is operating at relative low speeds, where coupling effects are considered to be negligible. Due to the above assumptions the kinematic and dynamic model of the vehicle is given by the equations below:

$$\dot{\check{\mathbf{n}}} = \check{\mathbf{J}}(\psi)\,\check{\mathbf{v}} \tag{2}$$

$$\begin{aligned} m_{11}\dot{u} &= -m_{22}vr + X_u u + X_{u|u|}u\,|u| + X \\ m_{22}\dot{v} &= m_{11}ur + Y_v v + Y_{v|v|}v\,|v| \\ m_{33}\dot{w} &= Z_w w + Z_{w|w|}w\,|w| + Z \\ J\dot{r} &= N_r r + N_{r|r|}r\,|r| + N \end{aligned} \tag{3}$$

where: $\check{\mathbf{n}} = [x\ y\ z\ \psi]^T$, $\check{\mathbf{v}} = [u\ v\ w\ r]^T$, m_{ii} is the ii'th entry of the vehicle's inertia matrix M, J is vehicle's moment of inertia about z axis, $X_k, X_{k\|k\|}$ where $k \in \{u, v, w\}$ are the linear and quadratic hydrodynamic coefficients in the surge, sway and heave directions respectively. The matrix

$$\check{\mathbf{J}}(\psi) = \begin{bmatrix} \cos\psi & -\sin\psi & 0 & 0 \\ \sin\psi & \cos\psi & 0 & 0 \\ 0 & 0 & 1 & 0 \\ 0 & 0 & 0 & 1 \end{bmatrix}$$

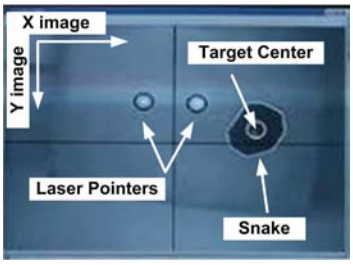

Fig. 1. Active Contours application

III. STATE ESTIMATION - UKF

As mentioned before the complete state vector of the vehicle is estimated by fusing data from the LVS and an IMU using an UKF. The LVS consists of a CCD camera and two laser pointers which are parallel to the camera axis. The LVS calculates the pose vector of the vehicle with respect to the center of a target which lays on the image plane. The target center and borderline are tracked using the Active Contours (Snakes) computer vision algorithm [8], which is implemented in the system software. Note that the center of the Snake in the image space (u_{tc}, v_{tc}) coincides with the center of the target (see figure 1).

The sensor model for the LVS is of the form:

$$\begin{bmatrix} u_{tc} \\ v_{tc} \\ L_1 \\ L_2 \end{bmatrix} = \mathbf{h}^{\alpha}\left(\check{\mathbf{n}}, \mathbf{w}^{\alpha}\right) \tag{4}$$

where L_1, L_2 are the ranges of each laser pointer from the surface the target is located and $\mathbf{w}^{\alpha}$ is zero mean white noise with covariance matrix $\mathbf{R}^{\alpha}$. The LVS is successfully used in previous works [4], [9], [6]. The analytical expression of eq. (4) and a more detailed description of the LVS can be found in [9].

The IMU used in this system (XSENS-MTi) provides 3D linear accelerations, 3D rate of turn and 3D orientation (Euler angles). The IMU weights only 50 gr and it is placed at the mass center of the vehicle aligned with its axes. The sensor model for the IMU that is implemented is of the form:

$$\begin{bmatrix} \hat{\psi} \\ \hat{r} \\ \hat{a_x} \\ \hat{a_y} \\ \hat{a_z} \end{bmatrix} = \mathbf{h}^{\beta}\left(\begin{bmatrix} \psi \\ r \\ a_x \\ a_y \\ a_z \end{bmatrix}, \mathbf{w}^{\beta}\right) \tag{5}$$

where $\mathbf{w}^{\beta}$ is a zero mean white noise with covariance matrix $\mathbf{R}^{\beta}$.

As described in the previous section, the equations describing the motion of the vehicle, as well as the equations describing the sensors are nonlinear. We choose to implement the Unscented Kalman Filter, which is a consistent estimator in order to calculate in real time the complete state vector of the vehicle:

$$\mathbf{p} = \begin{bmatrix} \check{\mathbf{n}}^T & \check{\mathbf{v}}^T & \dot{\check{\mathbf{v}}}^{\mathbf{T}} \end{bmatrix}^T$$

Note that the measurements from the IMU and LVS sensor arrive at different rates and especially for the LVS those

rates vary. In order to take into consideration the varying rate of the LVS sensor we need to appropriately shape our UKF fusion strategy. A multi-rate UKF was succesfully reported in [10]. Our approach is similar but we relax the assumption of constant rate measurement to produce an asynchronous fusion strategy. The system model that we implement is (2, 3), augmented with a 4-dimensional model for the accelerations to produce a 12-dimensional system model that is omitted in this paper for space considerations. The system model can be written as:

$$\dot{\mathbf{p}}(t) = \mathbf{f}(\mathbf{p}(t), \mathbf{U}(t)) + \mathbf{w}^m(t)$$

where $\mathbf{U}(t)$ is the input vector and $\mathbf{w}^m(t) \sim N(0, \mathbf{Q})$ is the process noise assumed to be zero mean white.

For the measurement model we have three different equations: the IMU measurement model eq. (5), the LVS measurement model eq. (4) and the IMU-LVS measurement model that is the augmentation of the two models, i.e.

$$\hat{\mathbf{y}} = \begin{bmatrix} \mathbf{h}^{\alpha}(\check{\mathbf{n}}, \mathbf{w}^{\alpha}) \\ \mathbf{h}^{\beta}(\check{\mathbf{n}}, \mathbf{w}^{\beta}) \end{bmatrix} \quad (6)$$

So at each iteration the fusion process actually uses only the sigma points corresponding to the sensor considered (i.e. the one that has produced the output at the current time instant) and the corresponding estimated output equation (i.e eq. (4) if only an LVS measurement was received, eq. (5) if only an IMU measurement was received, or eq. (6) if an LVS and an IMU measurement were received concurrently). Moreover, the algorithm uses the corrector equations with only the subset of the outputs dictated by the sensor to obtain the state estimation (see also [11],[10]): The estimation can be produced at the time instant it is needed by propagating the model up to that time instant.

IV. Controller Design

A. Polar-like Coordinates

The design approach we follow in this paper is to design our controller at the kinematic level and then backstep the kinematic controller into the dynamics of the system. A very convenient kinematic representation of our system for the purposes of controller design is the polar-like coordinates (Fig. 2):

$$\begin{aligned} \dot{e} &= -u\cos a + v\sin a \\ \dot{a} &= -r + u\tfrac{\sin a}{e} + v\tfrac{\cos a}{e} \\ \dot{\theta} &= u\tfrac{\sin a}{e} + v\tfrac{\cos a}{e} \\ \dot{z} &= w \end{aligned} \quad (7)$$

where $\mathbf{e}$ is the distance vector from the robot to the target, θ is the angle of $\mathbf{e}$ with the reference frame $< G >$. The origin of the reference frame is chosen to be the center of the inspection target and $a = \theta - \psi$ is the angle measured between the vehicle's principal axis and the distance vector $\mathbf{e}$.

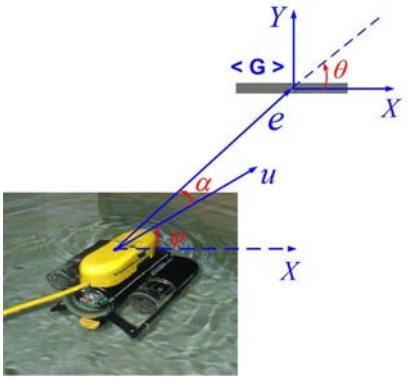

Fig. 2. Polar-like System

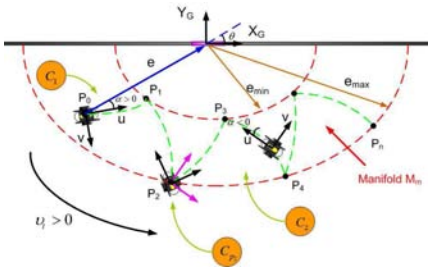

Fig. 3. Problem Statement. Vehicle performs a sawtooth-like trajectory inside manifold M_m, while keeping the target inside the field of view

B. Design at the Kinematic Level

Approach: The purpose of the proposed control scheme is to impose a bounded trajectory around the center of a target and inside manifold M_m, while guaranteeing that the target remains inside the camera's optical field, as shown in Fig.3. Due to the lack of actuation in the sway direction it is convenient to define the proposed control scheme initially at the kinematic level. Such a kinematic controller has been defined in our previous work [6]. The dynamic controller will be derived by feed-forwarding the dynamics (3) of the vehicle and back-stepping the kinematic controller into the dynamics of the system.

Since the controller design in the kinematic level follows the multi-mode control logic presented in our previous work [6] here we will only discuss portions of it. Basically the kinematic controller is broken down in the design of Linear and Angular Velocity Control Laws:

Linear Velocity Control Law: The purpose of this linear velocity control scheme, is to move the vehicle inside the boundaries e_{min} and e_{max} of manifold M_m (Fig. 3). When the vehicle reaches the lower bound e_{min} then the desired point of the controller is placed at e_{max} and vice versa. We have the following result:

Proposition 1: Assume the system (7). Then the control law

$$u = \frac{\gamma(t)(e - e_d) + v\sin a}{\cos a} \quad (8)$$

asymptotically stabilizes e at e_d as long as $|a| < a_0 <\neq \frac{\pi}{2}$ where a_0 a constant parameter and $\gamma(t)$ a user supplied positive gain.

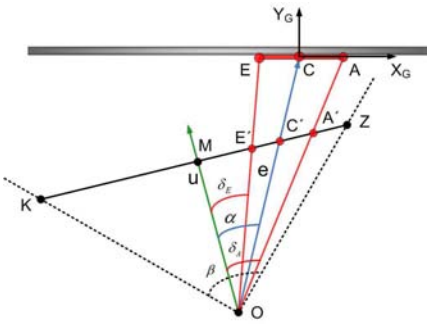

Fig. 4. Target projection on the image plane - Design of the angular velocity controller

Proof: Consider the following candidate Lyapunov function:

$$V_u = \frac{1}{2}(e - e_d)^2$$

The time derivative is: $\dot{V}_u = (e - e_d)\dot{e} \Rightarrow$
$\dot{V}_u = (e - e_d)(-u\cos a + v\sin a)$ Substituting the control on the time derivative of the Lyapunov function we get: $\dot{V}_u = -\gamma(e - e_d)^2 = -2\gamma V_u < 0$ which implies that the system is asymptotically stable at e_d since $\gamma(t) > 0$. ■

Implementation details: The joystick position υ_t defines the value of set point e_d to be either e_{min} or e_{max}, as well as the value of gain γ. Consider υ_t as the value describing the distance of the joystick axis from the center along its horizontal axis. When the user moves the joystick axis to the right $\upsilon_t > 0$, the vehicle must move to the right (positive cartesian y). In this case, if $\alpha < 0$, then $e_d := e_{max}$, otherwise, if $\alpha > 0$, then $e_d := e_{min}$. When the user moves the joystick axis to the left $\upsilon_t < 0$, the vehicle must move to the left (negative cartesian y). In this case, if $\alpha > 0$, then $e_d := e_{max}$, otherwise, if $\alpha < 0$, then $e_d := e_{min}$. The gain $\gamma(t) = |u_t|$. This gain regulates the robot velocity. Also note that the parameter a_0 always exists as long as the initial conditions are not at $|a| = \frac{\pi}{2}$.

Angular Velocity Control Law: The angular velocity controller is in fact responsible for keeping the target inside the camera's optical field. A similar controller was produced in our previous work [6], and more details can be found there. Referring to Fig. 4, the left most point of the target (point E) is projected to the location of E' of the image space and respectively the rightmost A at A'. Depending on the configuration of the vehicle, when $\alpha < 0$, the controller has to stabile A' at a desired distance $z_{d_{A'}}$ from the image center M. Respectively, when $\alpha > 0$ it has to stabilize E' of at the desired distance $z_{d_{E'}}$ from the image center M. The distances $s_1 = MA'$ and $s_2 = ME'$ have been calculated in [6] and they are functions of e, a, ψ, i.e. $s_1 = f(e, \alpha, \psi)$ and $s_2 = g(e, \alpha, \psi)$. We have the following result:

Proposition 2: Assume the system (7) and define mode C_1 when $a < 0$ and mode C_2 when $a > 0$. At mode C_1 apply the angular velocity control law:

$$r = \frac{-\frac{k}{2}(s_1 - z_{d_{A'}}) - \frac{\partial f}{\partial e}\dot{e} - \frac{\partial f}{\partial a}\dot{\theta}}{\frac{\partial f}{\partial \psi} - \frac{\partial f}{\partial a}} \tag{9}$$

and at mode C_2 apply the angular velocity control law

$$r = \frac{-\frac{k}{2}(s_2 - z_{d_{E'}}) - \frac{\partial g}{\partial e}\dot{e} - \frac{\partial g}{\partial a}\dot{\theta}}{\frac{\partial g}{\partial \psi} - \frac{\partial g}{\partial a}} \tag{10}$$

Then while in mode C_1 the system is exponentially stable at $z_{d_{A'}}$ and while in mode C_2 the system is exponentially stable at $z_{d_{E'}}$.

Proof: Same as in [6] ■

The controllers defined above will be successful in maintaining the target image in the field of view. However since we aim to produce a sawtooth like trajectory, we need some additional angular velocity controllers that will be able to transfer us between the modes C_1 and C_2 when reaching the upper and lower bounds e_{min} and e_{max}. To achieve this we introduce two additional modes: Mode C_{P_1} that can be activated when we are in mode C_2 and implements the angular velocity controller:

$$r = -k_{P_1}\left(s_1 - z_{d_{A'}}\right) \tag{11}$$

and mode C_{P_2} that can be activated when we are in mode C_1 and implements the angular velocity controller:

$$r = -k_{P_2}\left(s_2 - z_{d_{E'}}\right) \tag{12}$$

The above controllers are simple P-like controllers and are designed directly in the image space. k_{P_1} and k_{P_2} are positive constants.

Dynamic Controller Synthesis via Feedback Linearization and Back-stepping: The kinematic controllers developed in the previous discussion are not always capable of handling missions occurring in more difficult environments such as open sea, where waves, currents and tether appearance significantly affect vehicle's motion. Transforming the kinematic controllers into dynamic will greatly improve the behavior of the vehicle in such environments. We will start by transforming the kinematic controllers to dynamic for modes C_1, C_2

Using the following input transformation:

$$X = m_{22}vr - X_u u - X_{u|u|}u|u| + m_{11}U_X$$
$$Z = -Z_w w - Z_{w|w|}w|w| + m_{33}U_Z$$
$$N = -N_r r - N_{r|r|}r|r| + JU_r$$

The dynamic equations (3) are transformed to:

$$\dot{\tilde{\mathbf{v}}} = \begin{bmatrix} U_x \\ h(u, v, r) \\ U_z \\ U_r \end{bmatrix} \tag{13}$$

where $h(u, v, r) = \frac{m_{11}}{m_{22}}ur + \frac{Y_v}{m_{22}}v + \frac{Y_{v|v|}}{m_{22}}v|v|$. We have the following result:

Proposition 3: Assume system (2) with dynamics defined by (13). At mode C_1 apply the control law:

$$U_r = u_{r_{C1}} = \dot{r}_{C_1} + \frac{k}{2}(r_{C_1} - r) - \left(f - z_{d'_A}\right)\dot{f}_{\psi a} \tag{14}$$

and at mode C_2 apply the control law:

$$U_r = u_{r_{C2}} = \dot{r}_{C_2} + \frac{k}{2}(r_{C_2} - r) - \left(f - z_{d'_E}\right)\dot{f}_{\psi a} \tag{15}$$

where r_{C_1}, r_{C_2} the controllers defined in (9) and (10) respectively and $\dot{f}_{\psi a} = \left(\frac{\partial f}{\partial \psi} - \frac{\partial f}{\partial a}\right)$. Then while in mode C_1 the system is exponentially stable at $z_{d_{A'}}$ and while in mode C_2 the system is exponentially stable at $z_{d_{E'}}$.

Proof: As shown in Proposition 2 the kinematic subsystem can be stabilized with the controllers (9) and (10) with Lyapunov function[1] $V_0 = \frac{1}{2}\left(f - z_{d'_A}\right)^2$. Using a backstepping approach, we introduce the Lyapunov function candidate: $V = V_0 + \frac{1}{2}\left(r - r_{C_1}\right)^2$ Taking the time derivative of V, we have: $\dot{V} = \left(f - z_{d'_A}\right)\dot{f} + \left(r - r_{C_1}\right)\left(\dot{r} - \dot{r}_{C_1}\right)$. Since $f = f\left(e, a, \psi\right)$, for $\dot{f}$ we will have (after regrouping): $\dot{f} = \dot{f}_{ea} + r\dot{f}_{\psi a}$ where $\dot{f}_{ea} = \frac{\partial f}{\partial e}\left(-u\cos a + v\sin a\right) + \frac{\partial f}{\partial a}\left(u\frac{\sin a}{e} + v\frac{\cos a}{e}\right)$ and $\dot{f}_{\psi a} = \left(\frac{\partial f}{\partial \psi} - \frac{\partial f}{\partial a}\right)$.

Writing $r = r + r_{C_1} - r_{C_1}$ and substituting in $\dot{V}$, we get: $\dot{V} = \left(f - z_{d'_A}\right)\left(\dot{f}_{ea} + \left(r + r_{C_1} - r_{C_1}\right)\dot{f}_{\psi a}\right) + \left(r - r_{C_1}\right)\left(\dot{r} - \dot{r}_{C_1}\right)$. So $\dot{V} = \left(f - z_{d'_A}\right)\left(\dot{f}_{ea} + r_{C_1}\dot{f}_{\psi a}\right) + \left(r - r_{C_1}\right)\left(\dot{r} - \dot{r}_{C_1}\right) + \left(f - z_{d'_A}\right)\dot{f}_{\psi a}\left(r - r_{C_1}\right)$. Now observe that (see also the proof of Proposition 2) $\left(f - z_{d'_A}\right)\left(\dot{f}_{ea} + r_{C_1}\dot{f}_{\psi a}\right) = \dot{V}_0 = -kV_0$. Substituting the controller (14) we get that:

$$\dot{V} = -kV_0 - \frac{k}{2}\left(r_{C_1} - r\right)^2 = -kV$$

The same procedures stands for mode C_2. ∎

The control laws proposed in Proposition 3 compensates for any values of the input U_X as well as for any motion of the under-actuated DOF across the sway direction since their values are known to the controller.

The proposed controller gives us the freedom to design an arbitrary (continuous) control law for the U_X control input, in order to carry out the target inspection task according to the input from the human operator.

One result we need to note is:

Proposition 4: System

$$\dot{v} = \frac{m_{11}}{m_{22}}\zeta + \frac{Y_v}{m_{22}}v + \frac{Y_{v|v|}}{m_{22}}v\left|v\right| \tag{16}$$

where ζ is the input, is input-to-state stable

Proof: To show that system (16) is ISS stable, a necessary and sufficient condition is to show that it admits an ISS-Lyapunov function [12]. Consider the ISS Lyapunov function candidate:

$$V = \frac{1}{2}kv^2$$

Its time derivative will be: $\dot{V} = kv\left(\frac{m_{11}}{m_{22}}\zeta + \frac{Y_v}{m_{22}}v + \frac{Y_{v|v|}}{m_{22}}v\left|v\right|\right)$ Since $Y_{v|v|} < 0$ we have $\dot{V} \leq \frac{k}{m_{22}}\left(m_{11}v\zeta + Y_v v^2\right)$ and after some manipulation an using that $Y_v = -|Y_v|$, we get: $\dot{V} \leq \frac{k}{m_{22}}\frac{m_{11}^2}{|Y_v|}\zeta^2 - \frac{k}{m_{22}}\frac{|Y_v|}{2}v^2$ which is an ISS-Lyapunov function. ∎

We note that by setting $\zeta = ur$ in the above equation we get the dynamics of the underactuated subsystem.

[1]The presented proof is for mode C_1. A similar procedure is followed for mode C_2.

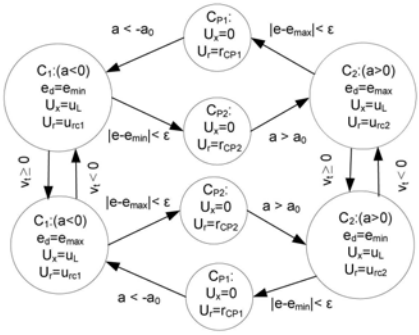

Fig. 5. State transition diagram

The importance of this result is that as long as the inputs to the underactuated subsystem (the product $\zeta = ur$) are bounded, the underactuated degree of freedom will be bounded. Moreover, as our input reduces to zero, the underactuated DOF will become stabilized to zero.

In the kinematic switching control scheme, controllers in modes C_{P_1} and C_{P_2} are responsible for the in-place rotation of the vehicle when it reaches the boundaries of manifold M_m. These controllers are now replaced by the equivalent dynamic controllers, by setting in Mode C_{P_1}: $U_r = r_{c_{p_1}}$ where $r_{c_{p_1}}$ the controller defined in (11) and by setting in Mode C_{P_2}: $U_r = r_{c_{p_2}}$ where $r_{c_{p_2}}$ the controller defined in (12).

C. Backstepping the linear motion controller

Proposition 5: Assume system (2) with dynamics defined by (13). The the control law:

$$U_x = u_L = \dot{u}_C + \frac{k}{2}\left(u_C - u\right) - \left(e - e_d\right)\cos a \tag{17}$$

where u_C the control law defined in (8) asymptotically stabilizes the system at e_d.

Proof: Choose as Lyapunov function candidate the function: $V = V_u + \frac{1}{2}\left(u - u_C\right)$. Take the time derivative: $\dot{V} = \left(e - e_d\right)\left(-u\cos a + v\sin a\right) + \left(u - u_C\right)\left(\dot{u} - \dot{u}_C\right)$ which can be written as $\dot{V} = \left(e - e_d\right)\left(v\sin a - \gamma\left(t\right)\left(e - e_d\right) - v\sin a\right) + \left(u - u_C\right)\left(\left(e - e_d\right)\cos a + \dot{u} - \dot{u}_C\right)$. Substituting the control law we get: $\dot{V} = -\gamma\left(t\right)\left(e - e_d\right) - \frac{k}{2}\left(u - u_C\right)^2 < 0$ ∎

D. Vertical Motion Control Law

The vehicle used in this work has a dedicated thruster for vertical motion. So the stabilization along the z axis is accomplished by feed-forward the dynamics along z axis and a simple PD position controller:

$$U_z = K_p e_z + K_d \dot{e}_z \;;\; K_p, K_d > 0 \tag{18}$$

where e_z the position error along z-axis and $\dot{e}_z$ its time derivative.To sum-up, Fig. 5 shows the control logic that is implemented.

V. EXPERIMENTS

In order to assess the overall efficiency of the system, a number of experiments were carried out. The experiments took place inside a water tank using a small underwater vehicle. The target of interest is located on an aluminium plate inside the tank. The ROV used is a 3-DOF (VideoRay PRO, VideoRay LLC, Fig.2), equipped with three thrusters, a control unit, and a CCD camera. The camera signal is acquired by a framegrabber (Imagenation PXC200). The LVS provides data asynchronously at $10 - 17Hz$ frequency. The laser pointers are equipped with Sony diodes, with 635 nm wavelength. The IMU is an XSENS MT-i and delivers data at $512Hz$. The joystick is a Microsoft Sidewinder Force Feedback 2.

A. Experimental Results

In order to prove the overall efficiency of the system, two experiments are presented. During the experiments the vehicle is kept at a constant depth using the PD controller mentioned in IV-D. The operator sets the vehicle's direction and speed using the joystick. In both experiments the direction was set from left to right, but in the first experiment the speed was adjusted by setting $\gamma = \upsilon_t = 10$, while in the second was set at $\gamma = \upsilon_t = 30$. As it can be seen from Fig.6 and Fig.7 the vehicle performs the desired sawtooth-like trajectory while keeps the target inside the vision field. The position of the most left s_1 and right s_2 points of the target borderline are always inside the boundaries (black lines) indicating the field of view limits. These limits come up from the cameras focal length, angle of view and the dimensions of the target. The time duration of the two experiments is exactly the same and it is obvious that when γ is larger (second experiment) the vehicle moves faster. The sign of angle α successfully changes, as it is imposed by the switching control scheme. Finally angle θ increases as the vehicle moves further along cartesian y axis. We can observe that in both experiments the trajectory of the vehicle is not quite smooth. This happens due to tether appearance which is not considered in our system. The tether is responsible for the well known drag effect, while constantly affects the responses of angles α and θ. Tether appearance will be part of the system model in our future work.

VI. CONCLUSIONS

In this paper we have developed a visual servoing control scheme for an underactuated underwater robot. The developed system provides a human operator the capability to move the vehicle around an inspection target without loosing the target from its field of view. The control system was developed at the kinematic level and using a backstepping methodology it was lifted to the dynamics of the robot. It was shown that the underactuated dynamics are input to state stable, and hence robust to bounded user inputs. An asynchronous fusion technique based on the Unscented Kalman Filter is proposed in this paper in order to effectively fuse data from a Laser Vision System and an Inertial Measurement Unit for tracking the robot motion.

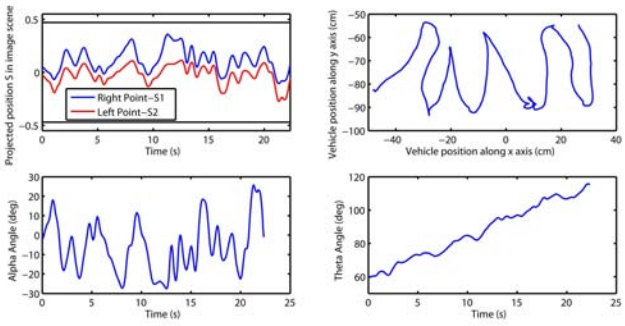

Fig. 6. First Experiment - $\gamma = 10$

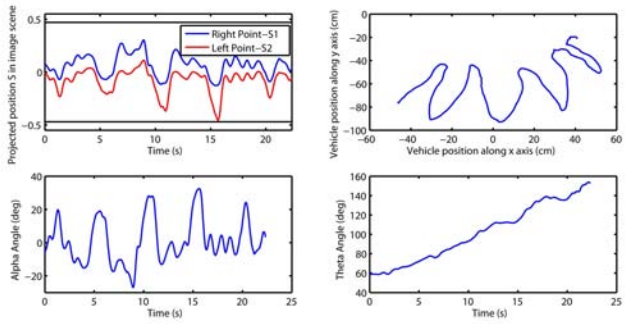

Fig. 7. Second Experiment - $\gamma = 30$

REFERENCES

[1] Y. Mezouar and F. Chaumette, "Path planning in image space for robust visual servoing," *Proc. of IEEE International Conference on Robotics and Automation*, pp. 2759–2764, 2000.

[2] B. Thuilot, P. Martinet, L. Cordesses, and J. Gallice, "Position based visual servoing: keeping the object in the field of vision," *Proc. of IEEE International Conference on Robotics and Automation*, pp. 1624 –1629, 2002.

[3] S. Bhattacharya, R. Murrieta, and S. Hutchinson, "Optimal paths for landmark-based navigation by differential-drive vehicles with field-of-view constraints," *IEEE Transactions on Robotics*, pp. 47–59, 2007.

[4] G. Karras and K. Kyriakopoulos, "Visual servo control of an underwater vehicle using a laser vision system," *Proc. of IEEE/RSJ Intelligent Robots and Systems*, pp. 4116–4122, 2008.

[5] P. Murrieri, D. Fontanelli, and A. Bicchi, "A hybrid-control approach to the parking problem of a wheeled vehicle using limited view-angle visual feedback," *The International Journal of Robotics Research*, pp. 437–448, 2004.

[6] G. Karras, S. Loizou, and K. Kyriakopoulos, "Semi-autonomous teleoperation of a non-holonomic underwater vehicle using a laser vision system: A visual-servoing switching control approach," *Proc of the 17th Mediterrannean Conference on Control and Automation*, 2009.

[7] T. Fossen, "Guidance and control of ocean vehicles," *Wiley, New York*, 1994.

[8] M. Kass, A. Witkin, and D. Terzopoulos, "Snakes: Active contour models," *International Journal of Computer Vision*, pp. 321–331, 1987.

[9] G. Karras, D. Panagou, and K. Kyriakopoulos, "Target-referenced localization of an underwater vehicle using a laser-based vision system," *MTS/IEEE OCEANS*, 2006.

[10] L. Armesto, S. Chroust, M. Vincze, and J. Tornero, "Multi-rate fusion with vision and inertial sensors," *Proc. of IEEE Conference on Robotics and Automation*, pp. 193–199, 2004.

[11] S. Julier and J. Uhlmann, "A new extension of the kalman filter to nonlinear systems," *Proc.of the Int. Symp. Aerospace/Defense Sensing, Simul. and Controls*, 1997.

[12] E. Sontag and Y. Wang, "On characterizations ofthe input-to-state stability property," *System and Control Letters*, pp. 351–359, 1995.